The effects of biomass syngas composition, moisture, tar loading and operating conditions on the combustion of a tar-tolerant HCCI engine (doi:10.1016/j.energy.2015.04.076)

S. Bhaduri[a], F. Contino[b], H. Jeanmart[a], E. Breuer[c]

[a] *Universite catholique de Louvain, Institute of Mechanics, Materials and Civil Engineering (iMMC), Louvain-la-Neuve, Belgium*
[b] *Vrije Universiteit Brussel, Department of Mechanical Engineering, Brussels, Belgium*
[c] *Breuer Technical Development, Malmedy, Belgium*

Abstract

Syngas, from biomass gasification, needs to be purified of condensible tars before being used as a fuel for spark ignition engines. A novel tar tolerant system is being developed, wherein a Homogeneous Charge Compression Ignition (HCCI) engine is fueled by impure syngas at intake temperatures above the tar dew point, thus avoiding the condensation of tars and its consequent problems. This paper introduces the novel concept and studies the sensitivities of HCCI combustion to key context relevant issues such as the variations in the combustible composition (H_2:CO ratio from 30:70 to 55:45 %), moisture (up to 12% by volume) and tars (from 3.5-17 g/Nm^3) at intake temperatures around 250°C. The effects of intake temperature (230-270°C) and pressure (1.0-1.2 bar) are also studied. The experiments are carried out with artificial syngas on a 435 cc mono-cylinder HCCI engine with a compression ratio of 12 and operated at 1500 RPM. Indicated efficiencies about 35% and Indicated Mean Effective Pressures about 2.5 bar were achieved at equivalence ratios between 0.3-0.34. In the tested ranges, moisture delayed the combustion while the effect of tars were insignificant.

Keywords: biomass, gasification, syngas, tars, water vapor, Homogeneous Charge Compression Ignition, HCCI

1. Introduction

Biomass gasification is a versatile process through which a variety of biomass can be converted into a gaseous fuel usable in Internal Combustion (IC) engines, steam boilers, etc. Combined Heat and Power (CHP) plants utilizing biomass gasification, in combination with IC engines, can deliver high efficiencies of conversion (up to 85% [1]) from the feedstock to energy and it is in this domain that the present work is relevant.

Raw "producer gas" or "syngas" from biomass gasification is composed of CO, H_2, CO_2, CH_4, N_2, water vapor, tars, particulate matter and other trace gases. One of the main challenges that hinder the commercial application of the biomass-gasification-IC engine chain concerns the issue of tars. Tars are hydrocarbons heavier than benzene which condense into liquid or solid forms at ambient conditions. Since, the conventional Spark Ignition (SI) engine requires the intake charge temperature to be well below 100°C for knock free operation, the hot syngas exiting from a gasifier (in the temperature range of 500 to 700°C) needs to be cooled down. The cooling process, while increasing the energy density of the syngas, results in the condensation of certain classes of tars, with their dew points being in the range of 200-250°C. The condensation of tars lead to the tar related problems of clogging and fouling of critical downstream components. Thus, in order to avoid/reduce recurring operational and maintenance problems, the filtration of tar becomes a necessary step in the cooling stage of a biomass gasification based power plant. The domain of tar filtration poses many complex issues such as filter inefficiencies, durability and maintenance of the purification systems along with environmental concerns arising from the disposal of the filtered tars or filtration media due to the toxic nature of tars [2].

To overcome the tar related problems, much of the research and development in the domain of biomass gasi-

Email addresses: subir.bhaduri@uclouvain.be (S. Bhaduri), francesco.contino@vub.ac.be (F. Contino), herve.jeanmart@uclouvain.be (H. Jeanmart), ernstbreuer@btd.be (E. Breuer)

fication can be classified into primary and secondary measures [3]. Primary measures focus on the development of better gasifier designs so as to reduce the production of tars within the gasifier, whereas, secondary measures focus on the destruction or filtration of tars downstream of the gasifier. The tar loading of the syngas depends on the type of gasifier and can range from 100 g/Nm^3 to as low as 20 mg/Nm^3 [4]. The latter low tar loading can be attributed to the effectiveness of primary measures such as the development of two-stage downdraft gasifiers. A review of such measures can be found in [3]. IC engines, on the other hand, pose stringent requirements on the syngas quality with tar loading <50 mg/Nm^3 [4]. The gap between the primary measures and the engine requirements have to be met by the secondary measures of tar purification, a review of which can be found in [5].

As an example of the challenges faced by primary and secondary measures, consider a modern two-stage downdraft gasifier of about 200 $kW_{thermal}$ capacity, installed at the authors' laboratory [6]. It is a scaled down version of a commercial 300 $kW_{electrical}$ NOTAR® industrial gasifier designed by Xylowatt s.a. of Belgium in collaboration with the Université catholique de Louvain. It produces a syngas with tar content less than 20 mg/Nm^3 as a consequence of primary measures which result in an improved gasifier design [7]. However, the syngas quality (tar content) fluctuates during transient operations, thus necessitating the use of secondary measures to ensure consistent syngas quality.

Given the challenges posed by the issue of tars, the objective of this paper is to present some studies related to an alternative and novel concept being developed at the authors' laboratory, which aims to make the IC engine section of the biomass-gasification-IC engine chain as "tar tolerant". If this is achieved, it would bypass or reduce the need of tar filtration altogether. This paper is divided into three broad sections. The first section provides a brief overview of the novel method which also includes a review of the relevant literature on HCCI engines operated on biomass syngas, along with listing the specific issues related to the concept and those which are a subject of this paper. The second section discusses the test-bench design and characteristics, experimental procedure and the post processing methodologies used for the experiments. In the final section, the experimental results are presented, followed by a concluding section.

2. HCCI engine fueled by unprocessed syngas - the novel concept

The problems related to tars can be reduced to problems related to tar condensation. Thus, a system can be developed where the average temperature of a tar loaded syngas is kept above the tar dew point, till the point of combustion. Bergman et al. classified the tar compounds into six main classes, with the class 5 tars dominating the tar dew point [8]. The dew point of class 5 tars at a concentration of about 1 g/Nm^3 was found to be about 250°C, and thus the investigations presented in this paper were carried around this value of intake temperature. Tars, being hydrocarbons, would eventually be consumed as part of the fuel in the combustion chambers of the engine. A suitable alternative to the SI engine, which can operate with such high intake temperatures, is the Homogeneous Charge Compression Ignition (HCCI) engine.

The HCCI engine combines the features of premixed homogeneous charge (fuel+air), as in a SI engine, with combustion driven by auto-ignition, as in a Compression Ignition (CI) engine. Since the pressure and temperature of the compressed charge is generally uniform throughout the combustion chamber volume, the autoignition occurs at multiple points, thus eliminating the need of typical flame-front driven stoichiometric combustion, found in the SI engine. This ability to operate at lean burn condition allows the HCCI operation to achieve low combustion temperatures which causes a subsequent decrease in Nitrous Oxide (NO_x) emissions. The HCCI engine also has the ability to be adapted to a wide variety of fuels and operating conditions. For an extensive review, the readers are referred to [9].

Biomass syngas as a fuel for SI engines has been explored by a number of authors, as reviewed in [10]. However, syngas as a fuel for HCCI engines has been explored only recently. A common issue studied in this domain concerns the coupling of real-time variations in the syngas composition to the inherently high sensitivity of HCCI combustion to the fuel chemistry. These syngas variations can be characterized in terms of variations in the volumetric concentration of H_2 and CO, represented in the form of H_2:CO share of the combustible part of the syngas. Variations in the inert components of syngas (N_2 and CO_2) also significantly influence the combustion through indirect means such as changing the ratio of specific heat of the charge mixture [11].

Yamasaki et al. found that the H_2 component of the syngas affects the HCCI combustion timing and heat release rates significantly, whereas the CO contributes to the overall performance due to its late combustion in

the cycle [12]. This was shown more conclusively, and with greater detail, through the use of CHEMKIN simulations and artificial syngas experiments, in a recent paper by Yamasaki and Kaneko [11]. Similar studies have been carried out by Haddith and Sobiesiak with a variation in the H_2/CO ratio from 29:71 to 57:43 [13]. Bika et al. used combinations of simplified syngas with H_2 and CO as the only components [14]. Achilles et al. compared the performance of an HCCI engine between a particular composition of syngas and natural gas and found that the both gases were comparable in performance in the ranges investigated [15]. In summary, the following characteristics can be observed regarding these works:

1. They were limited to Intake Temperatures (T_{in}) <200°C and compression ratio (τ) >20.
2. The objectives were to explore the HCCI engine as an alternative to the conventional SI engine, in the context of pure and cold syngas.
3. There was no mention of the possibility of high temperature HCCI operation for addressing the tar issues.
4. Only dry syngas mixtures were studied, which is typical in the case of cooled syngas.

The motivations, within which the studies of this paper have been conducted, differ from the aforementioned works due its focus on the high temperature HCCI combustion of syngas-air mixtures so as to be tar tolerant.

2.1. Challenges of the concept

In order to explore the viability of this concept, the following broad issues can be foreseen:

1. Testing the capability of tar tolerance.
2. Power de-rating.
3. Maturity of the HCCI technology.
4. Performance/Sensitivities of HCCI combustion to syngas characteristics and operating conditions.

Although, in principle, operation at high temperatures would avoid tar condensation, this ability could be challenged by the fact that operational constraints may require the engine body to be operated at much cooler temperatures, and thus may lead to some chances of deposition. Additionally, the subsequent destruction of tars through combustion may be hindered by pockets of incomplete combustion, which are a major cause of CO and HC emissions in a HCCI engine [16]. While, measurements of tar deposits would require experiments with long hours of operation with tar loaded syngas (for example see [17]), to assess the destruction of tars, Gas Chromatography/Mass Spectroscopy (GC/MS) measurements at the intake and the exhaust could be carried out. The high temperatures of combustion may also lead to the polymerization of tars into soot particles, which can add to emission concerns and thus must be accounted for.

The second issue of power de-rating is primarily because of the low calorific value of syngas and is also a matter of concern for SI engine applications using syngas[18]. Haggith et al. found that at low equivalence ratios, which is the domain of HCCI engines, the calorific values of syngas-air mixtures are comparable to those of fossil fuel-air mixtures [**?**]. However, in the present context, the effects of de-rating shall be more significant due to the high intake temperatures involved combined with the low knock-limited equivalence ratios, characteristic of the HCCI engines. The de-rating issue could be addressed using techniques such as Exhaust Gas Recirculation [19] or intake boosting [20], for example.

The third issue concerns the maturity of the HCCI technology, which as of today is instrument intensive due to the lack of any direct control on the combustion timing. The performance and control of HCCI combustion is often carried out using the costly and sophisticated in-cylinder pressure measurement systems, thus adding to the problems. HCCI engines also suffer from high sensitivities to operating conditions, combustion history, and other parameters, thus requiring careful monitoring.

All these issues are not in the scope of this paper or in the capability of the current experimental setup. However, work is under way to address the power de-rating issues using EGR, which will be the subject of a future paper.

2.2. Objectives of this paper

The objectives of this paper are limited to studying the performance and the sensitivities of HCCI combustion to a few key parameters, which would form a necessary base for the exploration of the research challenges discussed in the previous subsection. The factors explored in this paper concern the sensitivity and performance of the HCCI combustion in response to:

1. Variations in the H_2:CO ratio of syngas.
2. Syngas moisture content.
3. Syngas tar content.
4. Operational parameters of intake pressure, p_{in}, and temperature, T_{in}.

To bring out the main tendencies between the causes and their consequences, the experimental procedure must be characterized by repetition, reliability and precise control of the influencing factors. Hence, in this study, idealized syngas compositions with simplified additives (which simulate the moisture and tar impurities) have been used in an industrially non-relevant air cooled mono-cylinder engine, which allows for the flexibility of the experiments. Therefore, variations between the results presented here and those that may be attained in more realistic circumstances must be expected.

The performance of HCCI combustion has been evaluated in terms of parameters such as the Indicated Efficiency (IE), the Combustion Efficiency (CE), the Indicated Mean Effective Pressure (IMEP) and the emissions of NO_x and CO. To explore the combustion behavior following parameters were considered: CA50 which is defined as the Crank Angle Degree (CAD) associated with 50% of the fuel heat release, the combustion duration which is defined as the difference between the CA90 and the CA10 CAD positions corresponding to the 90% and the 10% of the fuel heat release in the cycle, and the Maximum Pressure Rise Rate (MPRR).

Based on the experimental requirements, an appropriate test bench and associated experimental procedure has been developed, as described in the next section. This is followed by a section describing the experimental results of this paper.

3. Experimental setup and methodology

HCCI combustion is sensitive to many parameters, of which the major ones are the compression ratio (τ), p_{in}, T_{in} and the fuel chemistry. The first subsection discusses the Computational Fluid Dynamics (CFD) studies carried out to determine the optimal engine and test bench characteristics, for experimenting in the current context. This is followed by a description of the test bench hardware, post processing methods used for analyzing the experimental data and uncertainty analysis.

3.1. Determination of main engine parameters

The main engine parameters were determined using CFD simulations based on the Tabulation of Dynamic Adaptive Chemistry (TDAC) method [21–24]. The main constraints considered in this context were the CA50, the MPRR and the maximum cylinder pressure. CFD analysis was used to evaluate these parameters as it outperforms zero dimensional models by taking into account the temperature inhomogeneities that result from heat transfers within the combustion chamber and thus leads to better estimates of the heat release rate and the ignition timing. Contino et al. have validated the current CFD model and methodology in various contexts and have shown that it can be used to predict the maximum pressure, the MPRR, as well as the ignition timing to a reasonable accuracy [21–24].

The mesh and simulation settings used in this context closely match the studies described in [23, 24]. The mesh was axisymmetric and counted around 20,000 cells at the Bottom Dead Center (BDC) of a 500 cc engine model. The turbulence model used was RNG k-ε. The kinetic mechanism[1] used to describe the combustion of syngas included 112 chemical species and 587 elementary reactions [25]. The simulations were performed at 1500 RPM to be relevant to the CHP context. A nominal syngas composition, from the two-stage gasifier in operation at the authors' laboratory, was chosen for the computations (see Table 3). A small portion (5%) of exhaust gases, consistent with the air fuel mixture, was included in the initial composition to represent the impact of trapped exhaust gases. A completely homogeneous mixture was assumed.

The objective was to observe the impacts of "input" parameters such as the τ, p_{in}, T_{in} and the syngas to air equivalence ratio, ϕ, on the specific "output" parameters of CA50, MPRR and the IMEP. For good cycle efficiency, CA50 limits were set between -5 to 10 CAD aTDC (after Top Dead Center) [26]. The MPRR, correlated to the engine knock, was constrained to a maximum of 10 bar/CAD. The maximum cylinder pressure of 100 bars was another of the constraints, but since the results never crossed 60 bar, this aspect was not analyzed further.

To begin with, the impact of engine geometry was considered. High MPRR and maximum pressures being characteristic of the HCCI engine, a diesel engine construction was assumed. The compression ratio, τ, was geometrically modified in the range of 10.5 to 13, while keeping the T_{in} at 250°C and ϕ at 0.5. As seen in Figure 1a the MPRR limit is crossed for τ >13. However, Figure 1b shows that the CA50 crossed the −5 CAD line much before at τ=11.7. Since the CA50 constraint is not rigid, the τ could be slightly higher, but must remain below 13 to respect the MPRR constraint.

The low Lower Heating Value (LHV) of syngas ($\approx$ 5 MJ/kg), the high T_{in} resulting in the low volumetric efficiency and the low values of ϕ expected from HCCI

[1] The kinetic mechanism is available by contacting the authors and can be downloaded from `http://veroniquedias.github.com/UCLouvain-Mechanism`

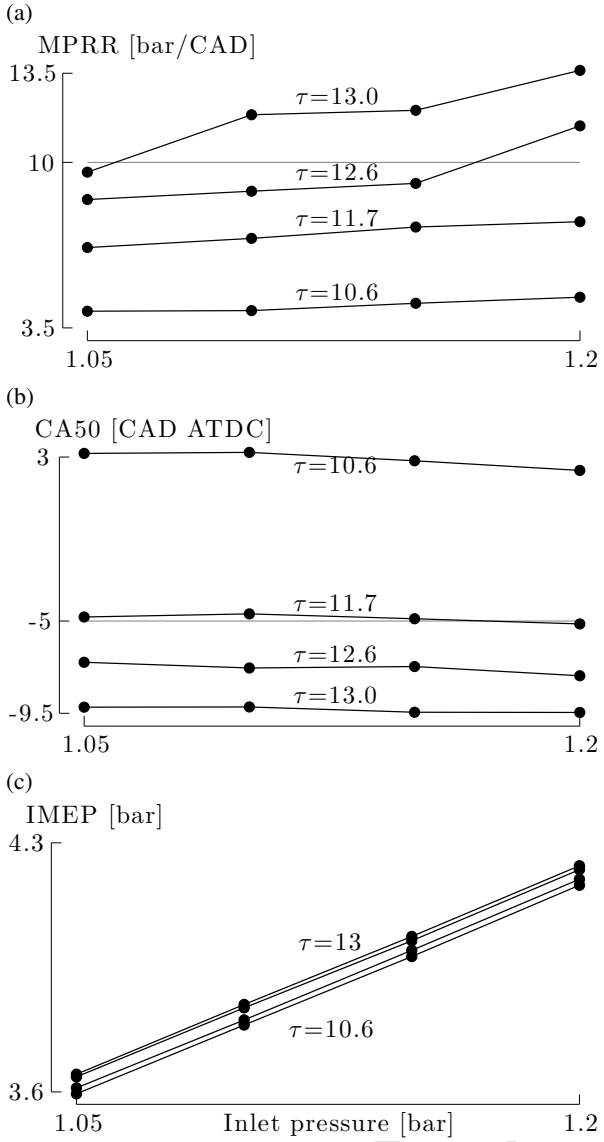

Figure 1: CFD studies of a 500 cc HCCI engine with pure and dry syngas as fuel while keeping T_{in} at 250°C and ϕ=0.5. The compression ratio τ effects the CA50 dramatically in Figure 1b which correspondingly results in increased MPRR as seen in Figure 1a. The IMEP however remains comparatively insensitive to the changes in the τ, as seen in Figure 1c. On the other hand p_{in} has a small impact on the CA50 in Figure 1b and a moderate impact on the MPRR in Figure 1a, except above the 10 bar/CAD threshold. The IMEP in Figure 1c is well correlated to the p_{in}.

operation would result in low IMEP values. Thus, in order to improve the IMEP, the effects of p_{in}, ϕ and the sensitivity to the T_{in} were evaluated.

In Figure 1 the effect of the p_{in} is investigated at each τ. Around τ=12, all constraints were found to be fulfilled for the whole range of p_{in} (see Figure 1b and Figure 1a) while having a positive impact on the IMEP in Figure1c. Thus the p_{in} could accordingly act as an efficient way to control the work output of the engine. On the other hand, an increase in the τ showed a low impact on the IMEP, arising mainly due to the better thermodynamic efficiency, while resulting in improper phasing (CA50) and high MPRR.

At ϕ=0.5, the results were already on the edge of the constraints and therefore, further increasing the equivalence ratio would not be an efficient way to improve the IMEP without using any other strategy to mitigate the corresponding rise in the MPRR. In fact, actual experiments presented in the following sections show that the MPRR limit is reached much before, with the ϕ of about 0.35. The value of T_{in}=250°C considered in this analysis is based on the assumption of the nominal tar dew point expected in general. However the tar dew point depends on various factors and can be lower, allowing for a lower T_{in} to be used. Simulating the engine at 230°C showed better IMEP due to the increase in the mass of fuel air mixture similar to an increase in p_{in}. Unlike the case of a higher p_{in}, reduction in the T_{in} also delayed the onset of the combustion which resulted in better ignition timing, lower MPRR and higher efficiencies. The effect of variations in the syngas composition was not considered in this part of the study.

Based on this CFD analysis, an engine with τ=12 was determined to be necessary along with a test bench system capable of delivering a variety of syngas compositions at the various p_{in} and T_{in} discussed above.

3.2. Experimental test bench

The schematic of the experimental setup is shown in Figure 2. Except for air, which is supplied from a compressor, all other gases are supplied from bottles. The flow of gases, including air, are controlled by Brooks thermal Mass Flow Controllers (MFC). The inert components of the mixture (air, N_2 and CO_2) are passed through a 2 kW electric heater that can raise the intake temperatures up to 270°C. The heated inert gases are mixed with the combustible gases (CO, H_2, and CH_4) in an appropriately sized drum which serves the dual purpose of creating a homogeneous mixture as well as dampening the pressure fluctuations of the mono-cylinder engine intake. Additives such as the tars and the water can be injected at the additives port before the mixing drum.

The specifications of the air cooled mono-cylinder engine and some experimental data are tabulated in Table 1. The engine was originally a diesel engine with its τ modified from 19 to the current 12. The piston combustion chamber was modified from a bowl shape to a

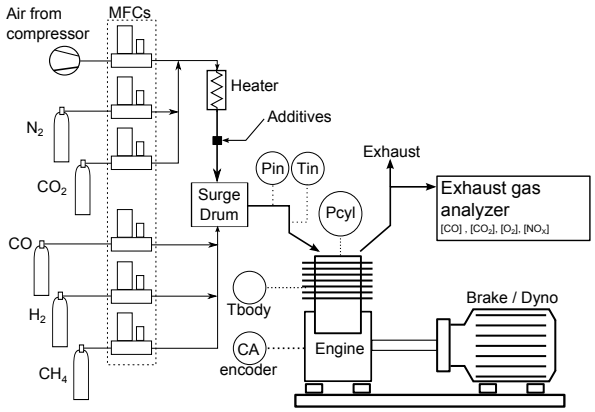

Figure 2: A schematic representation of the HCCI engine test bench.

Engine	Air cooled mono-cylinder
Displacement	435 cc
Compression ratio	12
Input valve closure	127° bTDC
Exhaust valve opening	127 ° aTDC
Bore	86 mm
Stroke	75 mm
RPM	1500
ϕ ranges	0.22-0.34
Mass Flow rate	$\approx$ 210 nL/min

Table 1: Specifications of the HCCI engine used in the experiments alsong with some experimental parameters.

flat design in order to minimize the heat losses by minimizing the surface area. The crevices were minimized to reduce the amount of un-burnt fuel. An electric motor controlled by a variable frequency drive controller acts as a brake / motor for the test bench.

The in-cylinder pressure is acquired by an AVL GH15D pressure sensor coupled to an AVL FlexIFEM charge amplifier. The pressure value is acquired for every 0.1 CAD triggered by a rotary encoder attached to the engine shaft. The T_{in} is measured near the intake port of the engine and is used as a feedback to the electrical heater for optimal regulation. The p_{in} is measured upstream of the intake manifold with additional care for dampening the pressure fluctuations of the engine intake. A Testo 350 M/XL Exhaust Gas Analyzer (EGA) is used to obtain O_2, CO_2, CO and NO_x emission measurements from the exhaust manifold. Hydrocarbon emission measurements were not carried out in these experiments due to the low concentration of CH_4 in the syngas. All the instruments are controlled by a National Instruments Compact Rio 9022 real-time controller. The acquisition and control is performed by an in-house code developed on the LabVIEW®p̃latform.

3.3. Experimental procedure and post-processing

Being an air-cooled engine, the cylinder body temperature during the experiments was kept at 110±5°C by manually adjusting the air intake of the inbuilt engine cooling fan. Experimental data were recorded when the CO emissions stabilized for each experimental point. Equivalence ratio sweeps were repeated three times in a random fashion, intermixed with different experimental points, so as to have an idea of the repeatability and the stability of the experiments. The plots presented in this paper depict all the experimental points with a line interlinking the means of the repeated experiments.

The TDC position of the engine was determined by the methods described in [27, 28] and is represented as 0 on the CAD scale. The in-cylinder pressure was pegged with p_{in} as a reference at the BDC position before compression. For each experimental point a sample of 100 consecutive cycles were acquired which were processed using the scheme elaborated in [29], resulting in a single mean filtered pressure trace. This pressure trace was analyzed by a zero dimensional combustion model, according to [30] using an algorithm elaborated in [31], to obtain the heat release (HR) rates. In these calculations, the blow-by and the crevice effects were neglected. The crank angle resolved values of the specific heat ratio, γ, were found using the JANAF polynomials while taking into account the species variations occurring during the combustion process. The heat losses from the cylinder walls were estimated by the Hohenberg heat transfer correlation, which is deemed suitable for the HCCI combustion [32]. The parameters of the Indicated Efficiency and IMEP were determined between the compression and expansion phases of the combustion stroke of the engine, and thus represent the gross instead of net values. The MPRR was calculated as an average of each of the 100 cycles of the sample after low pass filtering (Butterworth filter, 10 kHz cut-off) to remove the differentiation noises as well as other spurious signals.

3.4. Uncertainty analysis

The propagation of uncertainties, from the experimental parameters to the final ones, are summarized in Figure 3. The left hand side lists the various sources of uncertainty from the fundamental measurements which contribute to the uncertainties in the intermediate parameters such as the combustion chamber chemical composition and the in-cylinder pressure (see Appendix A). The uncertainties in these parameters in-turn affect

the final derived parameters listed on the right side of the figure. The uncertainty calculations carried out for the heat release and the CA50 (see Appendix B) assume the uncertainties in the specific heat ratio (γ) and the heat losses are negligible, compared to cylinder pressure uncertainties, and thus do not take them into account. To summarize, the maximum of the uncertainties, with 95% confidence levels, are reported for a few chosen parameters in the Table 2. Experimental results plotted in the next section are devoid of uncertainty indicators for the sake of clear representations.

The uncertainty in the CA50 estimation was observed to vary widely based on the CA50 value, with increased uncertainties for cases where the CA50 occurred much later than the TDC. However, as a note of caution, since the CA50 estimation is based on many assumptions (mass burn rate, heat losses and zero dimensional heat release analysis) coupled with the high uncertainties (originating mainly from uncertainties in the pressure sensor), its value is best interpreted in terms of trends rather than in absolute.

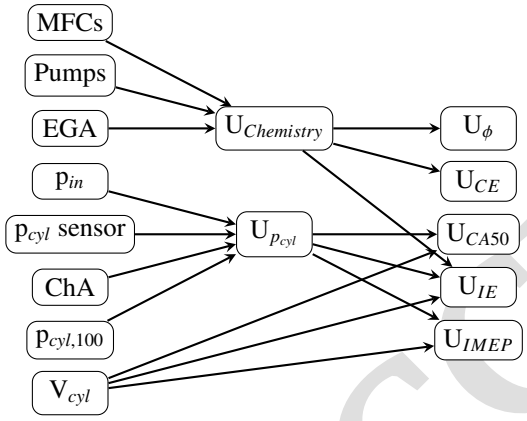

Figure 3: Propagation of uncertainty work flow. The new terms and notations are as follows: pumps for additive pumps (tars or water), p_{cyl} for in-cylinder pressure, ChA for the in-cylinder pressure Charge Amplifier, $p_{cyl,100}$ for the 100 cycle pressure traces and V_{cyl} for the in-cylinder volume. U stands for the resulting uncertainties with $U_{Chemistry}$ indicating the uncertainty in the charge chemical composition that affects the uncertainties in ϕ, U_{ϕ}, the Combustion Efficiency U_{CE} and the Indicated Efficiency U_{IE}.

4. Experimental results

The objectives of the experiments were to study the impact of charge compositions as well as the operational parameters, p_{in} and T_{in}, on the HCCI combustion. The charge composition is affected by the equivalence ratio ϕ, H_2:CO ratio, moisture content as well as the amount of tars in the syngas. The following sections discuss the experimental results obtained as a response to the aforementioned variations.

Parameters	Max U_{95}
ϕ_{in} [% rel.]	2
CE [% rel.]	3
CA50 [abs. CAD]	11.4
IE [% rel.]	10
IMEP [% rel.]	5.5
Tars [abs. g/Nm^3]	4
H_2O [abs. Vol.of syngas, %]	2.5

Table 2: Maximum U_{95} uncertainties of important parameters. The uncertainties in the CA50, tar concentrations and the moisture content are in their respective absolute values (abs.)while the others are expressed in relative percentages (rel.). The high uncertainty in the calculated CA50 indicates that this parameter must be interpreted for its trends rather than in absolute.

4.1. Variations in the dry and pure syngas composition

The syngas composition varies as a function of time for any gasifier which may cause fluctuations in the engine performance. In order to study the response of HCCI combustion to the compositional variations, experiments with three dry compositions, representative of the typical syngas from the two-stage downdraft gasifier at the authors' laboratory, were carried out. The tested compositions differed only in the H_2 and CO concentrations as listed in Table 3. In this sub-section, the effects of the influences of the H_2:CO proportion on the various combustion parameters are examined while the ϕ is changed from 0.22 to 0.34. Operational parameters, T_{in} and p_{in}, are held constant at 250°C and 1.2 bar respectively.

In Table 3, the low LHV of the dry syngas can be attributed to air being used as the gasifying agent. Thus, about 59% of the bulk syngas volume consists of inert components (N_2 and CO_2) which results in the low Lower Heating Value (LHV). The table also mentions the LHV of the stoichiometric mixture with air as well as the LHV of the mixture at ϕ=0.3 from which it can be concluded that for all practical purposes, the influence of the variations in the LHV due to the variations in the H_2:CO ratio, can be neglected.

Figure 4 shows the variations in the CA50 and the combustion duration, depicted as |CA90-CA10| in the figures, as a function of the equivalence ratio ϕ for the three compositions. The heat content of a combustion process is directly linked with the ϕ. Due to the critical dependency of autoignition processes on the temperature and the fuel chemistry, inhomogeneities in the thermal and species distribution throughout the compressed

	Molar fractions		
	Low	Nom.	High
H_2	0.12	0.18	0.22
CO	0.28	0.22	0.18
N_2	0.48	0.48	0.48
CO_2	0.11	0.11	0.11
CH_4	0.01	0.01	0.01
H_2:CO [%]	30:70	45:55	55:45
A/F_{stoic} [kg_{air}/kg_{fuel}]	1.14	1.21	1.26
LHV_{fuel} [MJ/kg]	4.34	4.52	4.65
$LHV_{mix,stoic}$ [MJ/kg]	2.03	2.04	2.05
$LHV_{mix,\phi=0.3}$ [MJ/kg]	0.90	0.90	0.89

Table 3: The three standardized dry syngas compositions used in the experiments are representative of the variations that can be observed in the typical use of the downdraft two-stage gasifiers. The first composition (Low) has a lower H_2CO ratio compared to the nominal composition (Nom.) which in turn has a H_2:CO ratio lower than the third composition (High).

volume cause the autoignition reactions to initiate only at certain favourable spots. These initial reactions, depending on the ϕ, influence the surrounding gas temperatures which in turn lead to further autoignitions and eventually a thermal runaway. Thus, as the ϕ increases, the autoignition processes accelerate, resulting in the reduction of the burn duration (see Figure 4b) along with an advance in the CA50 (see Figure 4a). On the other hand, the CO-rich syngas composition (H_2:CO=30:70) lagged behind in the trends of CA50 compared to the other compositions which are relatively H_2-rich. For example, at ϕ=0.28 the lag amounts to a large 3 CAD. This lag and its consequences, as shall be seen in the following sections, can be attributed to the differences in the rates of combustion of CO and H_2.

The HCCI combustion can be characterized by the auto-ignition delay times for the different species involved. As discussed in [33], the mixtures with higher H_2 content have shorter auto-ignition delays compared to mixtures with higher CO content. Thus, as seen in Figure 4, at low ϕ, the slow combustion of CO in the CO-rich syngas results in the correspondingly large combustion duration and late CA50. Due to the rapid expansion in the gas volume after the TDC, the resulting temperature drop decreases the combustion rate of CO rich syngas at low ϕ and eventually quenches it. On the other hand, for the H_2 rich syngas, the higher combustion rates result in the appropriate combustion phasing. Thus, a short combustion duration with the CA50 position near the TDC is necessary in order to avoid quenching.

The quality or completeness of combustion can be de-

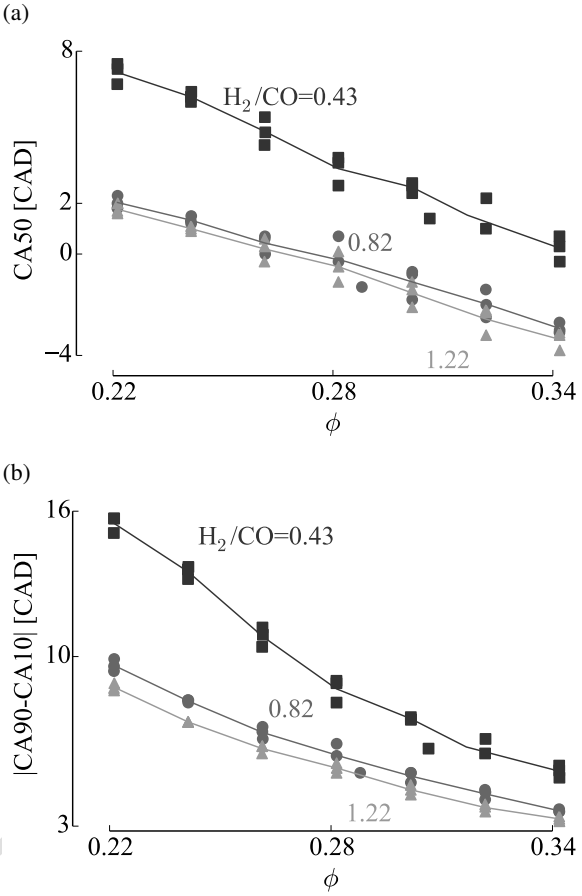

Figure 4: Variations in HCCI combustion as a function of ϕ for different H_2:CO mixture ratios. The CA50 of the 30:70 mixture lags behind the H_2 richer mixtures along with a much wider burn duration.

fined in terms of the Combustion Efficiency (CE):

$$\mathrm{CE} = \left(1 - \frac{\text{LHV of emissions}}{\text{LHV of intake}}\right) \times 100 \qquad (1)$$

The CE of the three compositions, as a function of the combustion duration |CA90-CA10| are shown in Figure 5a. As described previously, the combustion of CO rich syngas at ϕ=0.22 is quenched and subsequently a large portion of the fuel remains un-burnt. This results in the low CE of approximately 80%. As the |CA90-CA10| decreases due to the increase in the ϕ or in the H_2:CO ratio, the CE improves.

In the context of syngas as a fuel in HCCI engines, due to the absence of any significant quantities of hydrocarbons, the bulk of CO emissions can be linked directly to the un-burnt CO component of the original fuel (see Figure 5b). The similarity between the trends of the CO emissions and the combustion efficiency shows

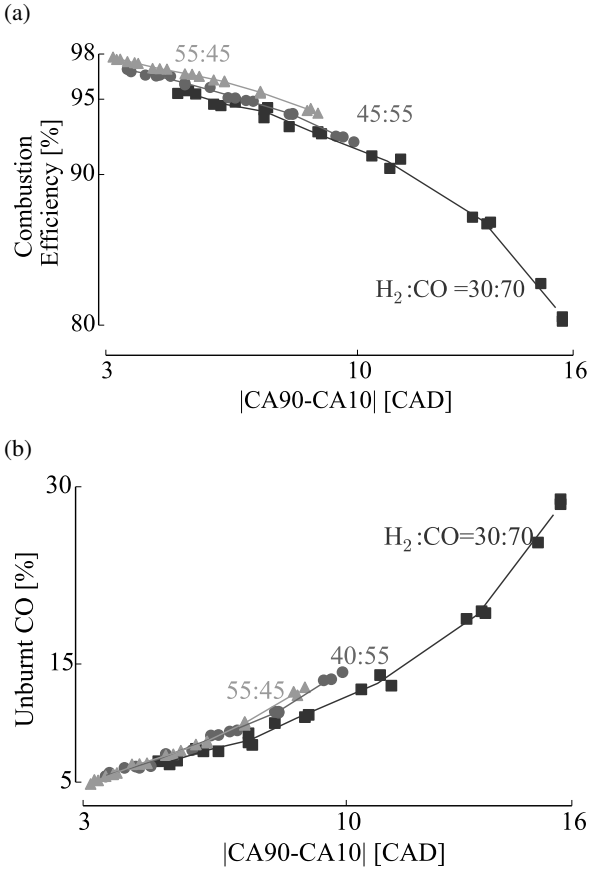

Figure 5: Combustion efficiency and unburnt portion of CO measured in the emissions as a function of the combustion duration |CA90-CA10| for various H_2:CO mixture ratios. Shorter burn durations caused by increasing ϕ are least affected by the quenching from volume expansion and hence have a better combustion efficiency with decreased emissions.

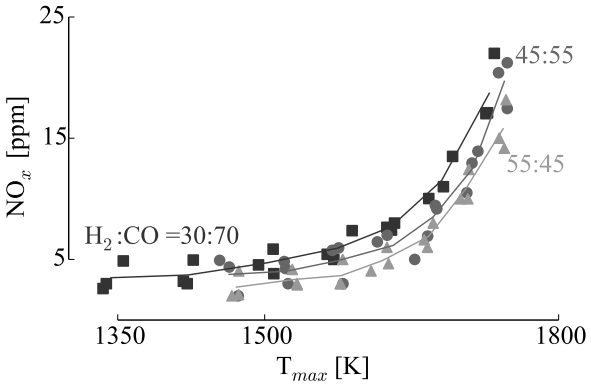

Figure 6: Experimental NOx measurements as a function of peak cycle temperature.

that a bulk of the inefficiencies are due to the slow burning CO component of the syngas fuel. As the combustion duration decreases due to the increase in ϕ, the CE moves beyond the 95% mark and the colder crevice regions become the dominant sources for the emissions according to [16]. Also, shorter combustion durations result in higher peak cycle temperatures, T_{max}, which increases the NO_x emissions as seen in the Figure 6. However, these emissions are still low compared to SI and CI engines due to the relatively cooler combustion temperatures, characteristic to the HCCI engines. On the other hand, the effects of H_2:CO ratio on the NO_x can be observed to be negligible.

Although the CE displays how much of the fuel has been burnt, the IE indicates how well the heat released by the fuel is converted into the pressure-volume work. The IE, as seen in Figure 7a, has a maximum when the CA50 is near the TDC. However, for the CO-rich syngas (H_2:CO=30:70), the IE maximum has a relatively higher value than the maximums from other compositions. This higher efficiency of the 30:70 mixture occurs at a relatively late CA50=2 CAD for a high $\phi \geq 0.30$. The resulting short combustion duration due to a high ϕ remains unaffected by the volume expansion, thus contributing positively to the overall cyclic work. On the other hand, for mixtures 45:55 and 55:45, since the CA50 is already near the TDC even at the low ϕ=0.22, the increase in the ϕ results in an increasing portion of the combustion occurring before the TDC. This results in a negative effect on the cyclic work due to the very high pressures coupled with the negative change in the volume during the compression phase. Thus the heat released is not well utilized resulting in a decrease in the IE, the peak of which occurs at the TDC for the H_2-rich compositions. As a summary, the combustion for optimal IE shall be such where a bulk of the combustion lies after the TDC, while the combustion duration remains short enough so as avoid the negative influences of volume expansion.

Figure 7b shows the increase in the IMEP as a function of the increasing amounts of fuel associated with higher ϕ. The higher IMEP for the CO-rich syngas at the ϕ=0.34 can be attributed again to the better combustion phasing, similar to the behaviour of IE.

The HCCI load range is limited by large variations between the cycles occurring at low ϕ and excessive MPRR, indicative of knock, occurring at higher ϕ. At low ϕ, HCCI combustion is spread over many crank angle degrees (large combustion duration) and thus highly sensitive to factors such as the cylinder wall temperatures and thermal inhomogeneities. Thus, as the wall

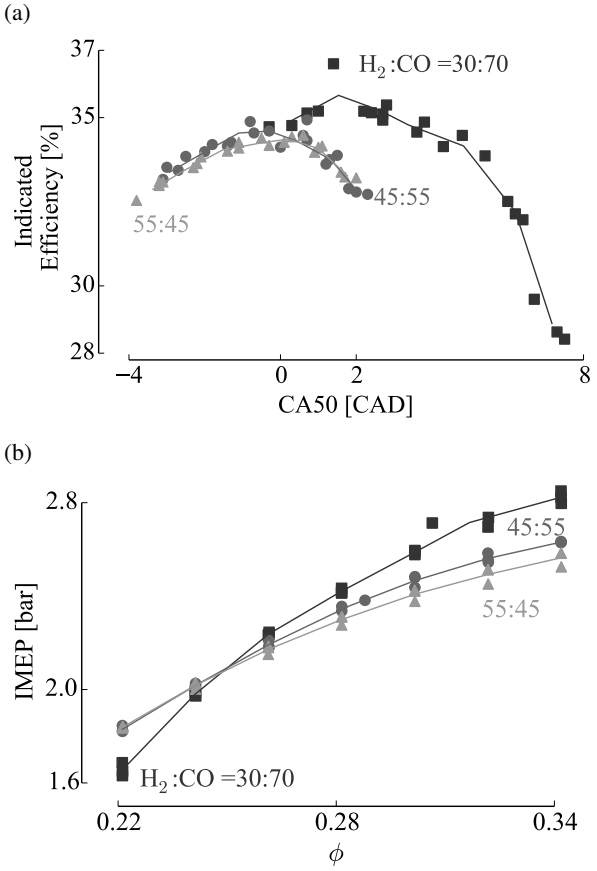

Figure 7: IE and IMEP as a function of CA50 for different H_2:CO mixture ratios. 7a) As the ϕ increases, the CA50 decreases with maximum IE occurring near and after the TDC. 7b) The IMEP improves with ϕ and is also responsive to the better combustion phasing of the 30:70 mixture.

temperatures are modified inconsistently by each cycle, the consecutive cycles are affected. The resulting variability between the cycles can be quantified in terms of the Coefficient of Variation (CoV_{IMEP}) in the IMEP computed for each cycle. An upper limit of 5 % in the CoV_{IMEP} is globally accepted as representing stable combustion [26]. The CoV_{IMEP}, plotted as a function of the combustion duration in Figure 8a, indicates the overall stability of the HCCI combustion throughout the experimented range. However, as the combustion duration increases, the CoV_{IMEP} increases, with the maximum increase corresponding to the case of the slow burning CO-rich syngas at ϕ=0.22.

On the other hand, as the ϕ increases, the shorter combustion duration produces high values of MPRR, as seen in Figure 8b. The MPRR is correlated to the knock phenomena and can therefore be utilized as a knock index with limits often determined through subjective operator experience [26]. In this case, a MPRR limit of 10 bar/CAD is found to be reasonable. The MPRR increase is accelerated with H_2-richness which can be attributed to the short ignition delays and fast H_2 reactions, as has been found by the other researchers in this domain [12–15]. Thus, the H_2 component increases the knock tendency of syngas and places an upper limit on the usable HCCI load range. On the other hand, the MPRR is lower for the 45:55 and 30:70 compositions even at the shortest combustion durations corresponding to the highest ϕ=0.34. Thus, the utilization of larger values of ϕ is possible with the CO-rich syngas as compared to the H_2-rich syngas which results in an improved performance in terms of the IE and IMEP.

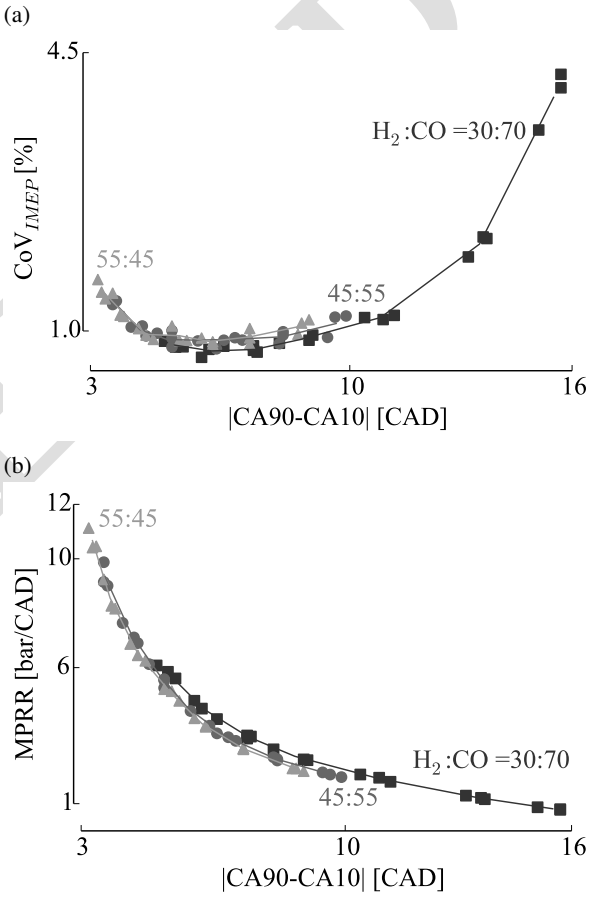

Figure 8: MPRR and CoV in the IMEP as a function of the combustion duration for different H_2:CO ratios. HCCI load range constraints of <5% CoV and <10 bar/CAD of MPRR is met by most of the test cases except for the H_2:CO mixture of 55:45 which crosses the MPRR limit at ϕ=0.34.

4.2. Effect of 'wet' syngas

Raw syngas from biomass gasifier contains approximately 10% of water by volume. Since the use of syngas in conventional IC engines has been concerned with cold, purified and dry compositions, the effects of moisture content on the engine performance has not been explored widely. However water as an additive has been studied in IC engines operated with conventional fuels for its anti-knock effects as well for reducing the NO_x emissions, (for example see [34]). In case of HCCI engines operated with conventional fuels, the objective of water injection has been to control the ignition timing by manipulating the rates of combustion as discussed in [35].

Since the objective of the current work is to function with raw syngas, the pure and dry syngas discussed in the previous section is moistened with water at varying proportions to simulate real case scenarios. A peristaltic pump has been used for injecting water into the hot gas flow just before the mixing drum so that the water is fully vaporised and is assumed to have become a part of the homogeneous fuel-air mixture. For the experiments, the syngas of nominal composition with H_2:CO=45:55 was chosen and the engine was operated at T_{in}=250°C and p_{in}=1.2 bar. Experiments were carried out at three ϕ values of 0.26, 0.30 and 0.34 while the volumetric percentage of water in the syngas was varied from approximately 4 to 12 %.

The main effect of water content in the fuel was found to be the reduction in combustion rates as seen in the Figure 9. As the water content is increased, the CA50 is retarded while the combustion duration (|CA90-CA10 |) increases significantly. Compared to the combustion phasing and duration of pure syngas (as seen in Figure 4) for the highest ϕ=0.34, the CA50 delays by more than 2 CAD when the water content increases from 0 to a low 4%. Due to the combustion delay caused by water, the combustion duration increases. The corresponding change in the CE can be seen in the Figure 10a where the decreasing trend is due to the twin effects of the drop in combustion temperatures caused by the water coupled by the increasing influence of the volume expansion due to larger combustion duration. The retarded CA50 also reduces the MPRR significantly. The MPRR value associated with neat syngas (at H_2:CO=45:55) at ϕ=0.34 (Figure 8b) reduced by more than 2 bar/CAD on the addition of only 4% water to the syngas.

With the increase in the water content of the syngas, minor improvements in the IE and IMEP were observed for ϕ=0.30, mainly due to the retarded phasing. The increasing delay of CA50 as well as the reduction in the MPRR due to increasing water content can allow operation at higher ϕ, resulting in an improvement in the overall performance. Similar effects can be found through the use of EGR in HCCI engines.

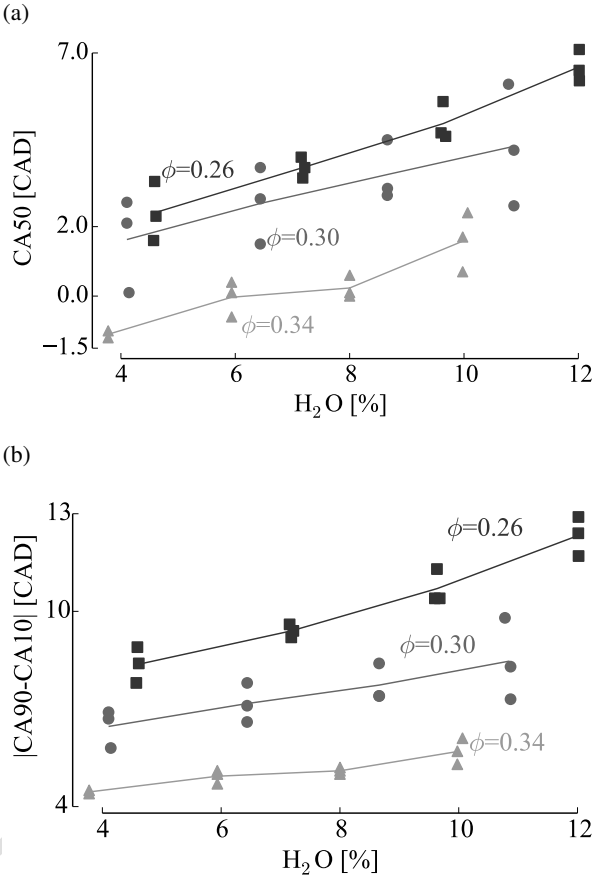

Figure 9: Effects of water content on the CA50 and burn duration for various ϕ. Water slows down the combustion processes which retards the CA50 and causes the combustion duration to increase.

4.3. Effect of Tars

The effect of the tars on the IC engines have not been sufficiently documented in the open literature. Hasler and Nussbaumer carried out some tests on the tar deposits formed in a SI engine after several hundred hours of operation with syngas containing tars <50 mg/Nm^3 [17]. Heavy tars, classified as those with boiling points higher than 200 °C were found having more tendency of forming deposits, compared to the comparatively lighter Polyaromatic Hydrocarbons (PAH) tars. As mentioned before in Section 2.1, the testing for tar depositions for the current setup are not feasible. However, on an immediate basis, the tar content in the syngas would alter the fuel chemistry due to its varying concentrations,

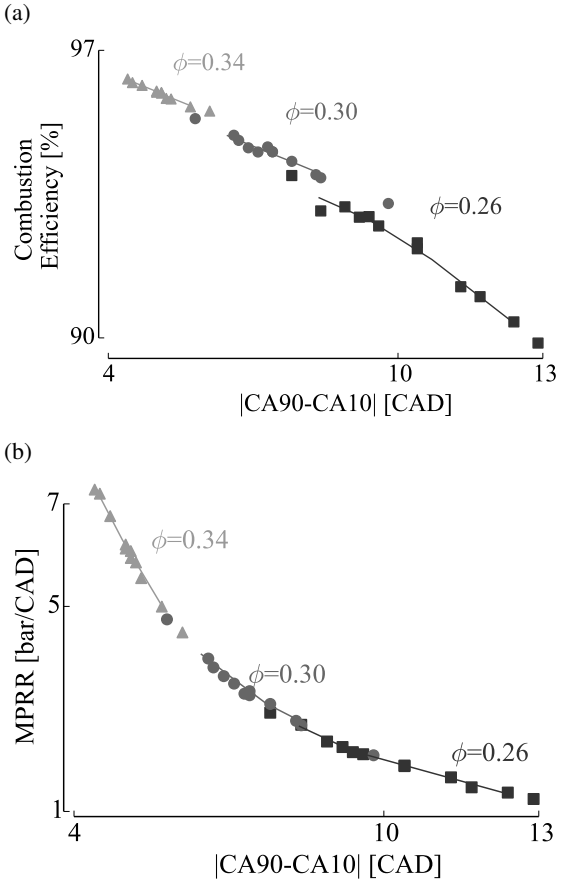

Figure 10: Effects of varying water content in syngas on the MPRR and the combustion efficiency for different ϕ. The MPRR decreases due to cooling effect of water while the combustion efficiency decreases due to the slow combustion resulting from the cooling effect and increased sensitivity to volume expansions

high LHV, influences on chemical kinetics, etc. Thus, instead of studies with a detailed tar composition, which is essential in the study of tar deposition, the amount of tars are of more relevance in the objectives of this paper. Amongst the wide variety of tar compounds found in the biomass syngas, naphthalene ($C_{10}H_8$) and toluene (C_7H_8) have been chosen as the representative tar compounds for the current set of experiments due to their significant proportions in the tar distribution and their wide acceptance as model tar compounds [36].

Naphthalene, being a solid at room temperature, was dissolved in toluene and a saturated solution was created with the solubility constant of M=2.635 mol/L. The quantities of the compounds were determined from the molar ratios known from the assumption of a saturated mixture. The mixtures were injected in the liquid form using a 10 ml syringe pump. The total tar (toluene+naphthalene) injection rates varied in the range of 3.5 g/Nm^3 to about 17 g/Nm^3 of syngas flow, which are much higher than the nominally expected 50 mg/Nm^3 from a modern two stage gasifier. The solution was injected before the surge drum in such a way so that the hot gases (which are above the boiling points of the tars in the solution) in the stream would vaporize the liquid droplets and produce a homogeneous mixture with the rest of the gases. The ϕ of pure syngas input was held constant at 0.3, while the injection rates of tars were changed.

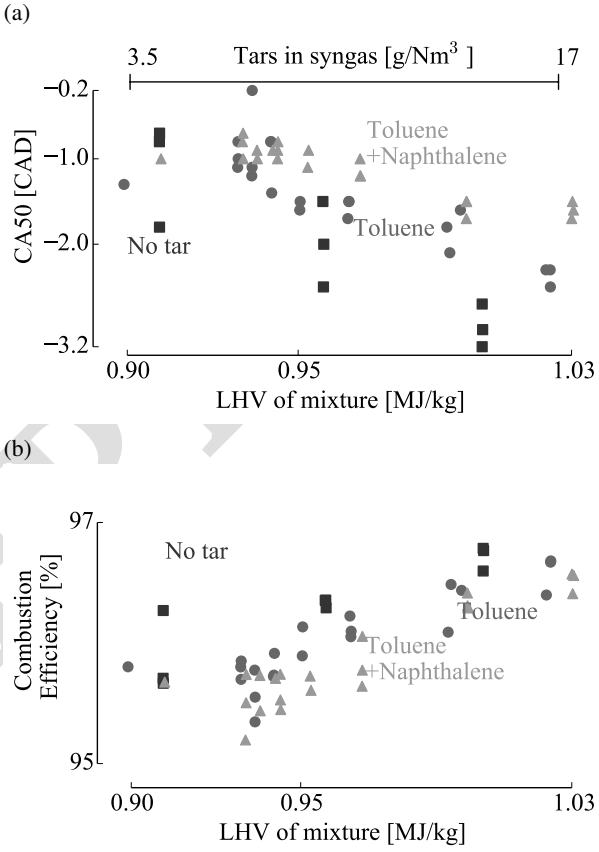

Figure 11: Effects of syngas tars on the CA50 and the combustion efficiency plotted as a function of the LHV of the syngas-tar-air mixture. The effects of naphthalene or toluene on the CA50 are comparatively lesser than pure syngas even at very large concentrations. The range of tars injected in terms of g/Nm^3 is indicated at the top in Figure 11a. The increasing CE indicates the burning of tars in the process.

The range of tars injected from 3.5 to 17 g/Nm^3 stands equivalent to a change in the ϕ of neat syngas with (H_2:CO=45:55) from 0.30 to 0.34. Figure 11a shows the changes in the CA50 due to the increasing LHV of the fuel and air mixture caused by the addition of tars. The figure also shows the corresponding

increases in the LHV for neat syngas achieved through increases in the ϕ. The combustion phasing seems to be most sensitive to the pure syngas, followed by the syngas containing pure toluene. The mixture of toluene and naphthalene shows the least effect on the CA50.

The results show that naphthalene, even in large quantities, does not dramatically alter the HCCI combustion behaviour. Modern two-stage gasifiers, such as the one at the authors' laboratory, produce approximately 20 mg/Nm^3 of tars instead of the minimum 3.5 g/Nm^3 used in the experiments. Thus, for all practical purposes, the effect of tars on the HCCI combustion can be neglected. The stability or mild increases in the CE (see Figure 11b), as a function of the increasing amount of LHV contribution due to the tars, can be assumed to be an indicator of the combustion of tars. However, detailed GC/MS measurements of the emissions would be needed to ascertain the proportion of un-burnt tars and thus comment on the tar destruction capabilities of such a system. In terms of performance, it is interesting to note that the addition of tars increased the LHV of the syngas while consequently causing a lesser advance in the combustion phasing, as compared to neat syngas. Thus higher tar content syngas could be beneficial to this application.

4.4. Effect of variations in p_{in}, T_{in}

For exploring the sensitivity of HCCI combustion to the variations in p_{in} and T_{in}, experiments were carried out for a fixed fuel composition at the nominal H_2:CO proportion of 45:55 and at three ϕ values of 0.26, 0.30 and 0.34. While exploring the sensitivity to p_{in}, the T_{in} was held constant at 250°C, whereas, while exploring the sensitivity to T_{in}, the p_{in} was held at a constant 1.2 bar.

An increase in the p_{in} results in larger compression temperatures and the fuel density, which accelerates the combustion leading to a corresponding advance in the CA50 as seen in Figure 12a. However, the resulting shorter combustion duration causes an increase in the MPRR (see Figure 12b). At ϕ=0.30, the MPRR (Figure 12b) increases by around 2 bar/CAD for an increase in the p_{in} from 1 to 1.2 bar. An increase in p_{in} results in an advanced CA50 beyond the TDC which negatively affects the IE as observed in 13a, however the effect is very small. On the other hand the IMEP increases steadily by about 0.3 bar as the p_{in} increases from 1.0 to 1.2 bar in Figure 13b. Thus the trends of p_{in} are similar to the ones predicted in section 3.1, however it must be noted that the CFD analysis was carried out at a much higher ϕ=0.5. Due to the increase in the IMEP, while having relatively smaller effect on the MPRR at ϕ=0.30,

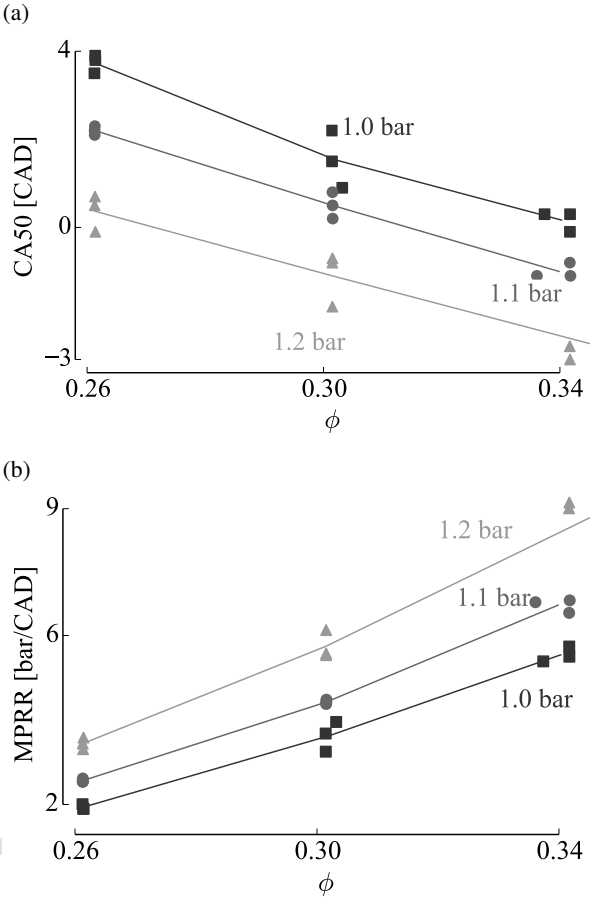

Figure 12: The CA50 and the MPRR plotted against ϕ for different p_{in}. A steady advance in CA50 can be seen as p_{in} is increased while the MPRR also increases.

a higher p_{in} could be used which indicates the potential for supercharging. However, this potential can only be exploited at ϕ where the combustion remains within the MPRR limit.

The T_{in} variations have a significant impact on the HCCI performance. The primary affect can be seen on the CA50 trends plotted in Figure 14a for different T_{in} of 230, 250 and 270 °C. For the high T_{in}=270°C, the autoignition processes begin well in advance of the TDC and are accelerated due to the volume compression, resulting in very short combustion durations and low CA50. As an example, at ϕ=0.30, an increase in the T_{in} by about 20°C from 230 to 250°C range advances the CA50 by about 8 CAD and in the 250 to 270°C range, by about 3.5 CAD. The corresponding increase in MPRR is about 1.5 and 0.5 bar/CAD respectively. While the IE in Figure 15a decreases for the T_{in} of 250 and 270°C as the ϕ increases, it increases for

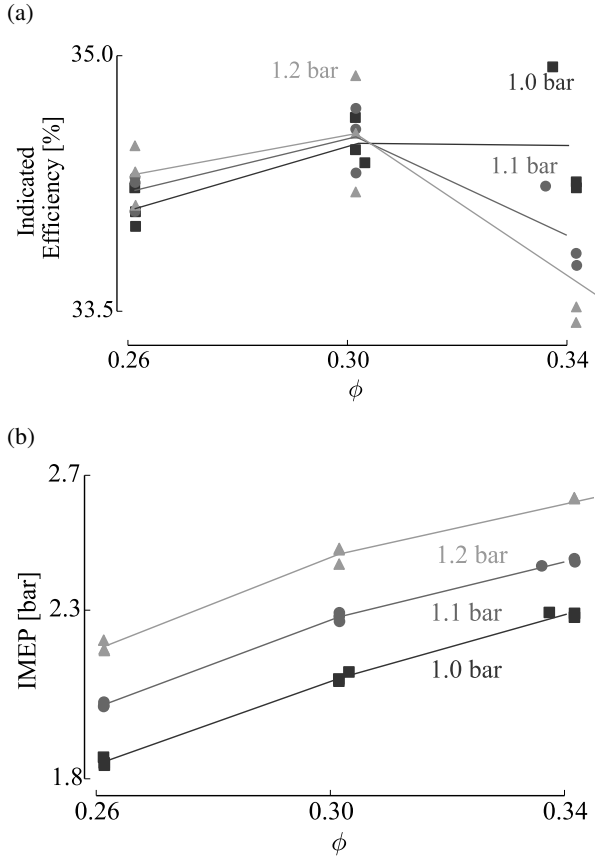

Figure 13: Effects of variation in the p_{in} on the IE and the IMEP at different ϕ. As p_{in} increases, the advance in the CA50 reduces the IE while the IMEP improves almost proportionally.

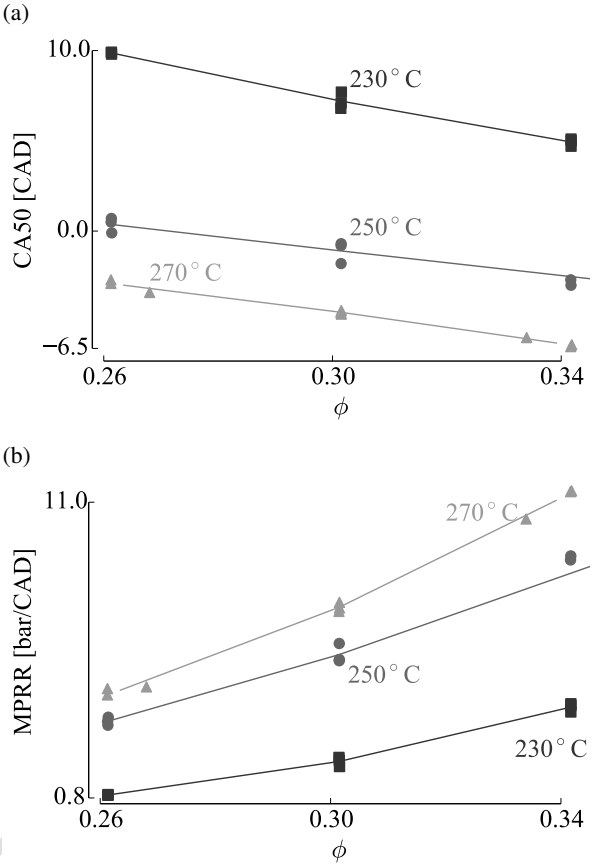

Figure 14: Effects of T_{in} on the CA50 and the MPRR for different ϕ. At lower T_{in}, the slow combustion results in late CA50 and low MPRR. At high T_{in}=270°C, the CA50 is too advanced giving rise to high MPRR.

the T_{in}=230°C. The higher efficiency of T_{in}=230°C at a later CA50 (at 5 CAD) is due to the combination of short combustion duration and the late combustion timing. The IMEP also improves due to the better phasing caused by the lower T_{in} as seen in Figure 15b.

The parameter T_{in} drastically affects the HCCI combustion, with better performance being achieved at lower temperatures. The lower limit of T_{in} however must be based on the tar dew point, which depends on the chemical composition as well as the concentration of the tars. The gasification setup upstream can be optimized for lower tar dew point without the constraint of tar quantities due to the increased tolerances inherent to this concept.

5. Conclusion

A novel method of dealing with the biomass syngas tars using an HCCI engine in combination with high temperature syngas has been introduced in this paper. Of the major challenges in the broader context, this paper covers experiments studying the HCCI combustion in response to various syngas compositions (including water and tars) as well as at various operating conditions of p_{in} and T_{in} using an artificial syngas supply in laboratory conditions. The key findings were:

- In terms of variations in the dry syngas composition, a CE >90% and an IE >35% were achieved for compositions of H_2:CO of 30:70, 45:55 and 55:45 for ϕ <0.35. The corresponding IMEP was above 2.5 bar.
- The maximum range of ϕ was limited to 0.34 due to the MPRR limits of 10 bar/CAD being crossed by the H_2-rich syngas (H_2:CO=55:45). Thus syngas with low H_2 content is preferred for better performance.

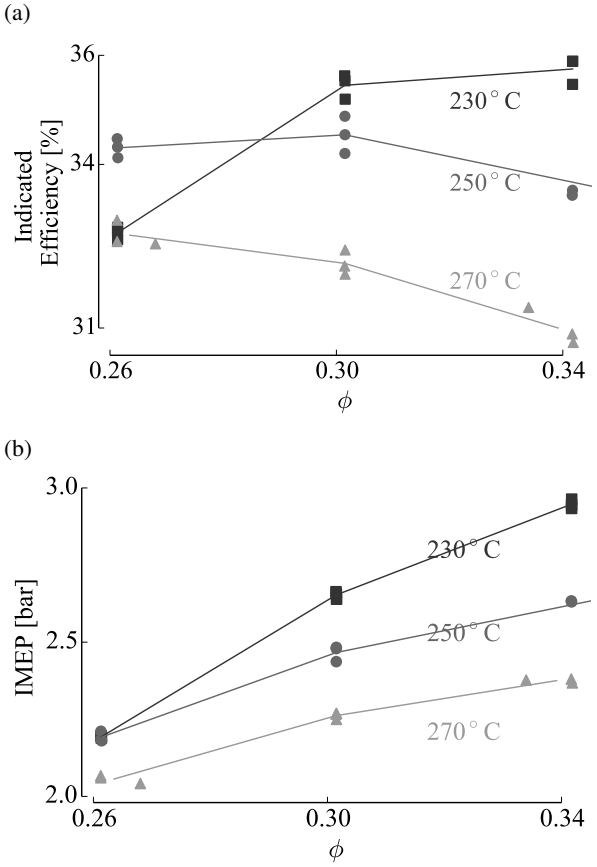

Figure 15: Effects of T_{in} on the indicated efficiency and the IMEP for different ϕ. At lower T_{in}, the better phasing and short combustion of ϕ=0.34 result in the high indicated efficiency and IMEP. As T_{in} increases, the bad phasing decreases both the indicated efficiency and the IMEP.

- HCCI combustion with wet syngas with varying proportions of moisture content showed positive effects resulting from delay in the combustion caused by the damping effect of water on the rate of chemical reactions. However, a slight penalty of a decrease in the CE was observed.

- Experiments with representative tar compounds of toluene and naphthalene, up to an unrealistically high 17 g/Nm^3, were carried out. Their effect on the HCCI combustion phasing was found to be negligible. However, the addition of tars increased the LHV without the detrimental effect of advancing in the combustion timing which was found in case of neat syngas.

- To improve the performance in terms of efficiencies and IMEP, higher p_{in} above 1.2 bar and lower T_{in} could be used. However, more research on the tar dew point needs to be carried out specific to the gasifier configuration in order to optimize the T_{in}.

The conclusions show the positive potential of this novel pathway. Work on the power de-rating aspects as well as the suitability of such a system with real syngas from a gasifier are being carried out by the authors and shall form the subjects of future papers. However, as discussed in the Section 2.1, a significant body of work concerning the key aspects of tar tolerance, power de-rating, suitability to various gasification designs along with improvements in the HCCI load limits and control strategies need to be carried out.

6. Acknowledgment

The research work described in this paper was funded by Service Public de Wallonie of Belgium under Project 'Gazo & Cie' for which we are greatly thankful.

References

[1] E. Bocci, M. Sisinni, M. Moneti, L. Vecchione, A. Di Carlo, M. Villarini, State of Art of Small Scale Biomass Gasification Power Systems: A Review of the Different Typologies, Energy Procedia 45 (2014) 247–256.

[2] J. J. Hernández, R. Ballesteros, G. Aranda, Characterisation of tars from biomass gasification: Effect of the operating conditions, Energy 50 (2013) 333–342.

[3] L. Devi, K. J. Ptasinski, F. J. J. G. Janssen, A review of the primary measures for tar elimination in biomass gasification processes, Biomass and Bioenergy 24 (2) (2003) 125–140.

[4] T. Milne, N. Abatzoglou, R. Evans, Biomass Gasifier Tars: Their Nature, Formation and ConversionNational Renewable Energy Laboratory, Tech. Rep. November, NREL (1998).

[5] P. J. Woolcock, R. C. Brown, A review of cleaning technologies for biomass-derived syngas, Biomass and Bioenergy 52 (2013) 54–84.

[6] H. Jeanmart, F. Bourgois, A. Bacq, X. Kuborn, Impact of the pyrolysis quality on the tar concentration of in the syngas, in: 16th European Biomass Conference & Exhibition - Proceedings, ETA-Florence Renewable Energies, Valencia,Italy, 2008, pp. 1–6.

[7] B. Berger, A. Bacq, H. Jeanmart, F. Bourgois, Experimental and Numerical Investigation of the Air Ratio on the Tar Content in the Syngas of a Two-Stage Gasifier, in: European Biomass Conference and Exhibition Proceedings, Lyon, France, 2010, pp. 20–25.

[8] P. C. A. Bergman, S. V. B. V. Paasen, H. Boerrigter, S. V. B. van Paasen, The novel OLGA technology for complete tar removal from biomass producer gas, in: Pyrolysis and Gasification of Biomass and Waste, Expert Meeting, Strasbourg, France, 2002.

[9] F. Zhao, T. W. Asmus, D. N. Assanis, J. E. Dec, J. A. Eng, P. M. Najt, Homogeneous Charge Compression Ignition (HCCI) Engines, Key research and development issues, SAE International, Warrendale, PA, 2003.

[10] F. Y. Hagos, a. R. a. Aziz, S. A. Sulaiman, Trends of Syngas as a Fuel in Internal Combustion Engines, Advances in Mechanical Engineering 2014 (2014) 1–10.

[11] Y. Yamasaki, S. Kaneko, Prediction of Ignition and Combustion Development in an HCCI Engine Fueled by Syngas, SAE Technical Paper 2014-32-0002.
[12] Yudai Yamasaki, Masanobu Kanno, Yasuhiro Taura, Shigehiko Kaneko, Study on biomass gas HCCI engine, SAE Technical Paper 2009-32-0066.
[13] D. E. Haggith, A. Sobiesiak, Effects of Fuel Composition Variations (H 2 :CO) for Biomass Gas HCCI Combustion, SAE Technical Paper 2012-01-1112.
[14] A. S. Bika, L. Franklin, D. B. Kittelson, Homogeneous charge compression ignition engine operating on synthesis gas, International Journal of Hydrogen Energy 37 (11) (2012) 9402–9411.
[15] M. Achilles, J. Ulfvik, M. Tuner, B. Johansson, J. Ahrenfeldt, U. Henriksen, F. X. Schauer, HCCI Gas Engine: Evaluation of Engine Performance, Efficiency and Emissions - Comparing Producer Gas and Natural Gas, SAE Technical Paper 2011-01-1196.
[16] S. M. Aceves, D. L. Flowers, F. Espinosa-Loza, J. Martinez-Frias, J. E. Dec, M. Sjöberg, R. W. Dibble, R. P. Hessel, Spatial Analysis of Emissions Sources for HCCI Combustion at Low Loads Using a Multi-Zone Model, SAE Technical Paper 2004-01-1910.
[17] P. Hasler, T. Nussbaumer, Sampling and analysis of particles and tars from biomass gasifiers, Biomass and Bioenergy 18 (1) (2000) 61–66.
[18] F. V. Tinaut, A. Melgar, A. Horrillo, A. Díez de la Rosa, Method for predicting the performance of an internal combustion engine fuelled by producer gas and other low heating value gases, Fuel Processing Technology 87 (2) (2006) 135–142.
[19] A. Bhave, M. Kraft, F. Mauss, A. Oakley, H. Zhao, Evaluating the EGR-AFR Operating Range of a HCCI Engine, SAE Technical Paper 2005-01-0161.
[20] J.-O. Olsson, P. Tunestå l, B. Johansson, Boosting for High Load HCCI, SAE Technical Paper 2004-01-0940.
[21] F. Contino, H. Jeanmart, T. Lucchini, G. D'Errico, Coupling of in situ adaptive tabulation and dynamic adaptive chemistry: An effective method for solving combustion in engine simulations, Proceedings of the Combustion Institute 33 (2) (2011) 3057–3064.
[22] F. Contino, T. Lucchini, G. D'Errico, C. Duynslaegher, V. Dias, H. Jeanmart, Simulations of Advanced Combustion Modes Using Detailed Chemistry Combined with Tabulation and Mechanism Reduction Techniques, SAE Int. J. Engines 5 (2) (2012) 185–196.
[23] F. Contino, F. Foucher, P. Dagaut, T. Lucchini, G. D'Errico, C. Mounaïm-Rousselle, Experimental and numerical analysis of nitric oxide effect on the ignition of iso-octane in a single cylinder HCCI engine, Combustion and Flame 160 (8) (2013) 1476–1483.
[24] F. Contino, J.-B. Masurier, F. Foucher, T. Lucchini, G. D'Errico, P. Dagaut, CFD simulations using the TDAC method to model iso-octane combustion for a large range of ozone seeding and temperature conditions in a single cylinder HCCI engine, Fuel 137 (2014) 179–184.
[25] V. Dias, C. Duynslaegher, F. Contino, J. Vandooren, H. Jeanmart, Experimental and modeling study of formaldehyde combustion in flames, Combustion and Flame 159 (5) (2012) 1814–1820.
[26] G. T. Kalghatgi, R. A. Head, Combustion Limits and Efficiency in a Homogeneous Charge Compression Ignition Engine, International Journal of Engine Research 7 (3) (2006) 215–236.
[27] M. Tazerout, O. Le Corre, S. Rousseau, TDC Determination in IC Engines Based on the Thermodynamic Analysis of the Temperature-Entropy Diagram, SAE Technical Paper 1999-01-1489 108 (4) (1999) 936–945.
[28] P. Tunestå l, TDC Offset Estimation from Motored Cylinder Pressure Data based on Heat Release Shaping, Oil & Gas Science and Technology – Revue d'IFP Energies nouvelles 66 (4) (2011) 705–716.
[29] F. Payri, P. Olmeda, C. Guardiola, J. Martín, Adaptive determination of cut-off frequencies for filtering the in-cylinder pressure in diesel engines combustion analysis, Applied Thermal Engineering 31 (14-15) (2011) 2869–2876.
[30] J. Heywood, Internal combustion engine fundamentals, McGraw-Hill, 1988.
[31] F. Contino, F. Foucher, C. Mounaïm-Rousselle, H. Jeanmart, Experimental Characterization of Ethyl Acetate, Ethyl Propionate, and Ethyl Butanoate in a Homogeneous Charge Compression Ignition Engine, Energy & Fuels 25 (3) (2011) 998–1003.
[32] H. S. Soyhan, H. Yasar, H. Walmsley, B. Head, G. T. Kalghatgi, C. Sorusbay, Evaluation of heat transfer correlations for HCCI engine modeling, Applied Thermal Engineering 29 (2-3) (2009) 541–549.
[33] J. J. Hernandez, C. Serrano, J. Perez, A. C. Jose, S. N. Cela, C. Real, Prediction of the Autoignition Delay Time of Producer Gas from Biomass Gasification, Energy & Fuels 20 (2) (2006) 532–539.
[34] R. Lanzafame, Water Injection Effects In A Single-Cylinder CFR Engine, SAE Technical Paper 1999-01-0568.
[35] M. Christensen, B. Johansson, Homogeneous Charge Compression Ignition with Water Injection, SAE Technical Paper 1999-01-0182.
[36] C. Li, K. Suzuki, Tar property, analysis, reforming mechanism and model for biomass gasification—An overview, Renewable and Sustainable Energy Reviews 13 (3) (2009) 594–604.
[37] Bipm.org, Evaluation of measurement data – Guide to the expression of uncertainty in measurement, Tech. Rep. September, BIPM (2008).
[38] G. T. Chin, J. Y. Chen, V. H. Rapp, R. W. Dibble, Development and validation of a reduced DME mechanism applicable to various combustion modes in internal combustion engines, Journal of Combustion 2011.

Appendices

A. Uncertainty in in-cylinder pressure

For determining the pressure uncertainty, a very simple model can be considered, where a change in the pressure Δp_{true} inside the cylinder develops a corresponding charge on the piezoelectric pressure sensor (PZT) through a sensitivity coefficient S_{PZT}. This charge is transferred to the Charge Amplifier (ChA) with a pre-programmed sensitivity coefficient S_{ChA} that converts it back into a pressure output Δp_{ChA}. Thus, the pressure signal from the amplifier can be expressed in a simplified form as:

$$\Delta p_{ChA} = \Delta p_{PZT} \cdot \frac{S_{PZT}}{S_{ChA}} \tag{A.2}$$

The Charge Amplifier can be assumed to function as an integrator of the sequential pressure changes which

results in the final measured output value. Although the amplitude of the amplifier output matches the amplitude of pressure change, the relevance of the change to the real pressure requires a known reference pressure. Thus, a pegging procedure is required which adds a constant reference pressure to the output, resulting in the final pressure:

$$p_{final,j} = \sum_{i=0}^{j} \Delta p_{ChA,i} + p_{peg} = p_{ChA,i} + p_{peg} \tag{A.3}$$

The true pressure is related to the final pressure as $p_{true} = p_{final} + \epsilon_{final}$ where ϵ stands for potential errors. The ϵ_{final} is a result of multiple error sources such as, piezoelectric sensor non-linearity (NL), thermal shock (TS), cyclic temperature drift (TD), changes in the transducer sensitivity over the calibrated sensitivity $S_{PZT,Cal}$ due to the material temperature changes (TSC), the non-linearity of the charge amplifier and the error in the pegging procedure (peg). Thus the equation becomes:

$$\begin{aligned} p_{final} + \epsilon_{final} =& (p_{final} + \epsilon_{PZT,NL} + \epsilon_{PZT,TS} + \epsilon_{PZT,TD}) \\ & \times \frac{S_{PZT,Cal} + \epsilon_{S,PZT,TSC}}{S_{ChA}} + \epsilon_{ChA,NL} \\ & + p_{peg} + \epsilon_{peg} \end{aligned} \tag{A.4}$$

The sensitivities of the transducer and the amplifier are set the same, thus $S_{PZT,Cal} = S_{ChA}$. Assuming the product of error terms are negligible, the equation can be simplified as:

$$\begin{aligned} p_{final} + \epsilon_{final} \approx& p_{final} + \epsilon_{PZT,NL} + \epsilon_{PZT,TS} + \epsilon_{PZT,TD} \\ & + p_{final} \frac{\epsilon_{S,PZT,TSC}}{S_{ChA}} + \epsilon_{ChA,NL} \\ & + p_{peg} + \epsilon_{peg} \end{aligned} \tag{A.5}$$

Thus, the uncertainty in the pressure data due to instrument error sources is:

$$u_{p,final} = \sqrt{\begin{aligned} & u^2_{PZT,NL} + u^2_{PZT,TS} + u^2_{PZT,TD} + \\ & \left(\frac{p_{final}}{S_{ChA}} u_{S,PZT,TSC}\right)^2 + u^2_{ChA,NL} + u^2_{peg} \end{aligned}} \tag{A.6}$$

The uncertainties due to thermal shock can be neglected in the current setup where the loads are very low. Also, the drift in the sensitivity due to the thermal effects have been neglected due to cyclic compensation provided by the charge amplifier. The uncertainty $u_{p,final}$ accounts only for the uncertainties originating from the pressure transducer-amplifier combination, and represents the *Type B* uncertainties [37]. The cyclic pressures are recorded for 100 consecutive cycles and thus a *Type A* uncertainty can be estimated. For k being the cycle number varying from 1 to N, the standard uncertainty in the mean pressure trace, $\bar{p}$, of the N cycles sample can be written as:

$$u_{p,\theta,Type\,A} = \sqrt{\frac{\sum (p_{\theta,k} - \bar{p}_\theta)^2}{N(N-1)}} \tag{A.7}$$

Thus, the final combined uncertainty in the in-cylinder pressure trace can be expressed as:

$$u_{p,\theta} = \sqrt{u^2_{p,\theta,Type\,A} + u^2_{p,Type\,B}} \tag{A.8}$$

B. Uncertainties in the heat release and the CA50

The uncertainty analysis of CA50 is not very common. This procedure develops on the one presented in the supplementary material of [38] by incorporating the variations in the specific heat ratio, γ, into the calculations.

This uncertainty analysis of the heat release assumes that the uncertainties over in-cylinder gas temperatures and thus the γ on one hand and the convective heat losses, on the other, are negligible. The rate of heat release, based on the First Law of thermodynamics, as a function of γ, p and instantaneous cylinder V is written as:

$$\frac{dQ}{d\theta} = \frac{\gamma}{\gamma - 1} p \frac{dV}{d\theta} + \frac{1}{\gamma - 1} V \frac{dp}{d\theta} \tag{B.9}$$

In order to avoid noise originating from the numerical differentiation of the pressure p, the following simplification is used:

$$\begin{aligned} \frac{d(PV)}{d\theta} &= P\frac{dV}{d\theta} + V\frac{dP}{d\theta} \\ \frac{dQ}{d\theta} &= \frac{1}{\gamma - 1}\frac{d(PV)}{d\theta} + P\frac{dV}{d\theta} \end{aligned} \tag{B.10}$$

Due to the discrete data, the cumulative heat release, Q, must be evaluated in terms of finite sums, i.e.

$$\Delta Q_i = \frac{1}{\gamma_i - 1} \Delta(P_i V_i) + P_i \Delta V_i \tag{B.11}$$

Therefore, the Q at a certain point j, between the Start of Combustion(SOC) and the End of Combustion (EOC)

can be written as:

$$Q_j = \sum_{i=SOC}^{j} \Delta Q_i \tag{B.12}$$

Finally, the uncertainty in the cumulative heat release takes the form:

$$u_{Q_j} = \sqrt{\sum_{i=SOC}^{j} u_{\Delta Q_i}^2} \tag{B.13}$$

Where...

$$u_{\Delta Q_i}^2 = (\frac{1}{\gamma_i - 1} u_{\Delta(p_i V_i)})^2 + (p_i \cdot u_{\Delta V_i})^2 + (\Delta V_i \cdot u_{p_i})^2$$

$$u_{\Delta(pV)_i}^2 = \frac{1}{4}\left[\begin{array}{l} (V_{i+1} \cdot u_{p_{i+1}})^2 + (p_{i+1} \cdot u_{V_{i+1}})^2 \\ + (V_{i-1} \cdot u_{p_{i-1}})^2 + (p_{i-1} \cdot u_{V_{i-1}})^2 \end{array} \right]$$

The CA50 is associated with the $Q50$, which is the 50% energy of the complete heat release, expressed as:

$$Q50 = 0.5 \cdot (Q_{max} - Q_{min}) \tag{B.14}$$

Therefore, the uncertainty in the $Q50$ is:

$$u_{Q50} = 0.5 \sqrt{u_{Q_{max}}^2 + u_{Q_{min}}^2} \tag{B.15}$$

Where the uncertainties in the Q_{max} and Q_{min} are readily obtained from the u_Q of the equation (B.13). Finally, the uncertainty in the CA50 is defined as the difference between the crank angle associated with the quantity $Q50$ (CA50) and that associated with the heat quantity $Q50 + u_{Q50}$:

$$u_{CA50} = CA_{Q50+u_{Q50}} - CA_{CA50} \tag{B.16}$$